



## GEOSCIENCES

# Variability in wet and dry snow radar zones in the North of the Antarctic Peninsula using a cloud computing environment

FILIFE D. IDALINO, KÁTIA K. DA ROSA, FERNANDO L. HILLEBRAND, JORGE ARIGONY-NETO, CLAUDIO WILSON MENDES JR & JEFFERSON C. SIMÕES

**Abstract:** This work investigated the annual variations in dry snow (DSRZ) and wet snow radar zones (WSRZ) in the north of the Antarctic Peninsula between 2015-2023. A specific code for snow zone detection on Sentinel-1 images was created on Google Earth Engine by combining the CryoSat-2 digital elevation model and air temperature data from ERA5. Regions with backscatter coefficients ( $\sigma^0$ ) values exceeding -6.5 dB were considered the extent of surface melt occurrence, and the dry snow line was considered to coincide with the -11 °C isotherm of the average annual air temperature. The annual variation in WSRZ exhibited moderate correlations with annual average air temperature, total precipitation, and the sum of annual degree-days. However, statistical tests indicated low determination coefficients and no significant trend values in DSRZ behavior with atmospheric variables. The results of reducing DSRZ area for 2019/2020 and 2020/2021 compared to 2018/2018 indicated the upward in dry zone line in this AP region. The methodology demonstrated its efficacy for both quantitative and qualitative analyses of data obtained in digital processing environments, allowing for the large-scale spatial and temporal variations monitoring and for the understanding changes in glacier mass loss.

**Key words:** Antarctic Peninsula Ice-sheet, cloud computing environment, CryoSat2, radar glacier zones, Sentinel-1, snowmelt.

## INTRODUCTION

The Antarctic Peninsula (AP) is the region of the Antarctic continent that presented the highest increase in oceanic and atmospheric temperatures, being the most sensitive portion to climate change (Costi et al. 2018, Lee et al. 2017, Mendes Jr et al. 2022). The geographical location and unique configuration of AP pose significant challenges to conducting *in situ* measurements of events related to atmospheric changes. The atmospheric warming recorded in this region reached between 2.5 °C and 3.0 °C since the second half of the 20th century (Turner et al. 2005, Steig et al. 2009, Costi et al. 2018, Tuckett

et al. 2019), causing important changes in the dynamics of the region. These changes have a direct impact on the loss of glacial area in the AP, which configures it as one of the regions of the continent with the highest values of negative mass balance (Mouginot et al. 2014, Sutterley et al. 2014, Rignot et al. 2019).

Active and passive microwave data from remote sensors are used to map variations in surface behavior over the AP, as well as climate reanalysis data on monthly, weekly, and daily scales (Zhou & Zheng 2017, Mendes Jr et al. 2022). Several studies utilizing microwave radiometers and scatterometers (specifically brightness temperature - Tb) as well as Synthetic Aperture

RADAR (SAR) data (focused on the backscatter coefficient -  $\sigma^{\circ}$ ) have been conducted to estimate variations in glacier facies in the region (Arigony-Neto et al. 2009, Zhou & Zheng 2017, Mendes Jr et al. 2022). These studies leverage the distinctive characteristics and capacities inherent in these archival datasets.

Compared to radiometer and scatterometer images, SAR images exhibit high spatial resolution, allowing for studying snowmelt patterns, glacial facies, and the snow line in detail (Rau et al. 2001, Rau & Braun 2002). The dry snow line (DSL), located close to the highest parts of glaciers, represents the lower boundary of the dry snow radar zone (DSRZ), separating this portion of the glaciers where no melting occurs from areas with frequent or occasional melting (Zhou et al. 2021), known as the percolation zone (PZ) and wet snow radar zone (WSRZ).

Due to its good spatial resolution and acquisition mode, SAR data, in conjunction with atmospheric climate reanalysis models, can be used to derive the position of the DSL and the variation in extent of radar glacier zones (Zhou & Zheng 2017, Zhou et al. 2021). Using three mosaics of RADARSAT ScanSAR images, Rau & Braun 2002 accurately demonstrated the potential to identify the boundaries between the DSRZ and PZ or WSRZ. Arigony-Neto et al. (2009) compiled a series of SAR images from ERS1/2 and ENVISAT to extract the altitude variation of the DSL in the AP, and the boundaries between the other snow zones over the period 1992-2005. Liang et al. (2021) used Sentinel-1 SAR in EW mode, with a 40m resolution, to extract freeze and thaw information from continental-scale time series.

Factors such as improved spatial resolution, shorter data acquisition intervals, and increased processing power in SAR data can synergistically enhance the precision and accuracy of these analyses. With the twin satellites of the Sentinel 1 (S1) mission, SAR data have become an even

more attractive alternative for radar studies of wet and dry snow surface zones, as this mission provides free C-band SAR imagery at 10, 20, and 40-meter (m) spatial resolution and revisit times of up to six days (ESA 2012, Buchelt et al. 2022). SAR data from S1 are sensitive to wet snow and can be applied for its mapping mainly during the ablation season (Malenovský et al. 2012).

Despite the advances, S1 data also have restrictions in the acquisition, including a residual noise called speckle. Speckle is inevitable in SAR images and can be removed using different methods in pre-defined windows, such as Lee 1980 and Frost et al. 1982. Other characteristic effects can be identified in SAR products, such as RADAR shadows, layover, and foreshortening (Rau & Braun 2002, Arigony-Neto et al. 2009, Mendes Jr et al. 2022) are related to the acquisition geometry of RADAR sensors, and require additional processing to solve these problems. On the other hand, a significant improvement facilitating the utilization of S1 data is the introduction of the S1-GRD collection. Level 1 Ground Range Detect (GRD) products consist of focused SAR data that has been detected, analyzed, and projected to ground range using a terrestrial ellipsoid model (ESA 2021). Ground range coordinates are the slant range coordinates projected onto the ellipsoid of the Earth. Pixel values represent detected magnitude. Phase information is lost. The resulting product has approximately square spatial resolution and square pixel spacing with reduced speckle due to the multi-look processing (ESA 2021).

Analyzing these parameters at a regional scale, such as in the AP, requires large amounts of data and an intensive processing routine in high-quality environments with large storage spaces, making the process slow and difficult. To address this problem, Big Earth Data (BED) computing platforms, such as Google Earth Engine

(GEE), offer new opportunities for research and analysis of snow melt in Antarctica, as they are ideally suited to handle scale variations and the complexities of spatiotemporal data (Gorelick et al. 2017, Wang et al. 2020, Liang et al. 2021).

GEE combines a multi-petabyte catalog of satellite imagery and geospatial datasets with planetary-scale analysis capabilities (GEE 2022). The platform has powerful geospatial analysis abilities and supports parallel computing to accelerate operations. Thus, processing time can be drastically reduced compared to local processing (Li et al. 2018). With the tools available on platforms like GEE, the processing of images and data from different sources at a regional scale, without the need for large storage bases, and with rapid retrieval of results for analysis, is now a reality.

Taking into account these aspects and resources, this paper aims to: i) extract both wet and dry snow zones on the ice sheet in the north of the AP, north of 65.20°S from S-1 images, using a processing script built on the GEE platform; ii) investigate the area variation of dry snow and wet snow zones between austral winters (June, July and August) and summers (December, January and February) in the 2015-2023 period; and iii) verify the influence of average superficial air temperature and annual precipitation on the obtained results.

## MATERIALS AND METHODS

### Study area

The study area comprises the AP continental region, at latitudes north of 65.20°S (Figure 1), and is located within the North Bioregion of the AP (Lee et al. 2017). This area the northernmost portion of the continent, which has an area of 17,000.00 km<sup>2</sup> and is the region that has experienced the greatest atmospheric warming, the highest area loss in recent decades (Mouginot

et al. 2014, Sutterley et al. 2014, Costi et al. 2018, Rignot et al. 2019, Tuckett et al. 2019). Glacial mass loss on the Antarctic continent will lead to the emergence of around 2,100 and 17,267 km<sup>2</sup> of new ice-free areas by the end of this century, with the upper limit representing almost 25% of the total area. Over 85% of these new ice-free areas will appear in the North Bioregion (Lee et al. 2017).

The AP is the northern portion of the continent, and is surrounded by the Bellingshausen and the Weddell seas. It is about 1,500 km long, extending almost longitudinally between latitudes 63° S and 75°S, being composed of an internal plateau with a mean elevation of 1,500 m. Its width varies from 35 km in the far north to almost 300 km at latitude 75°S (Mendes Jr et al. 2022).

This peninsula had strong and statistically significant warming over the last 60 years (Jones et al. 2019). Among other consequences, this increase in temperature caused significant changes in glacial systems of the Antarctic Peninsula, such as the decrease of seasonal sea ice, increasing trend in melting events, retreat of glacier fronts, and break-up and disintegration of ice shelves (Scambos et al. 2000, Cook & Vaughan 2010, Trusel et al. 2012, Bevan et al. 2020, Mendes Jr et al. 2022). The persistent and intense meltwater fluxes contributed to accelerate the retreat of Antarctic Peninsula ice shelves, as reported by Scambos et al. (2000), Van den Broeke (2005), Trusel et al. (2013), Bevan et al. (2020) and Mendes Jr et al. (2022). These losses currently contribute to global sea level rise (The IMBIE team 2018).

### Dataset

In this study, we used image data from the Sentinel-1 (S1) mission, provided by a 5.405 GHz dual-polarization C-band SAR instrument, and processed as Level-1 Ground Range Detect

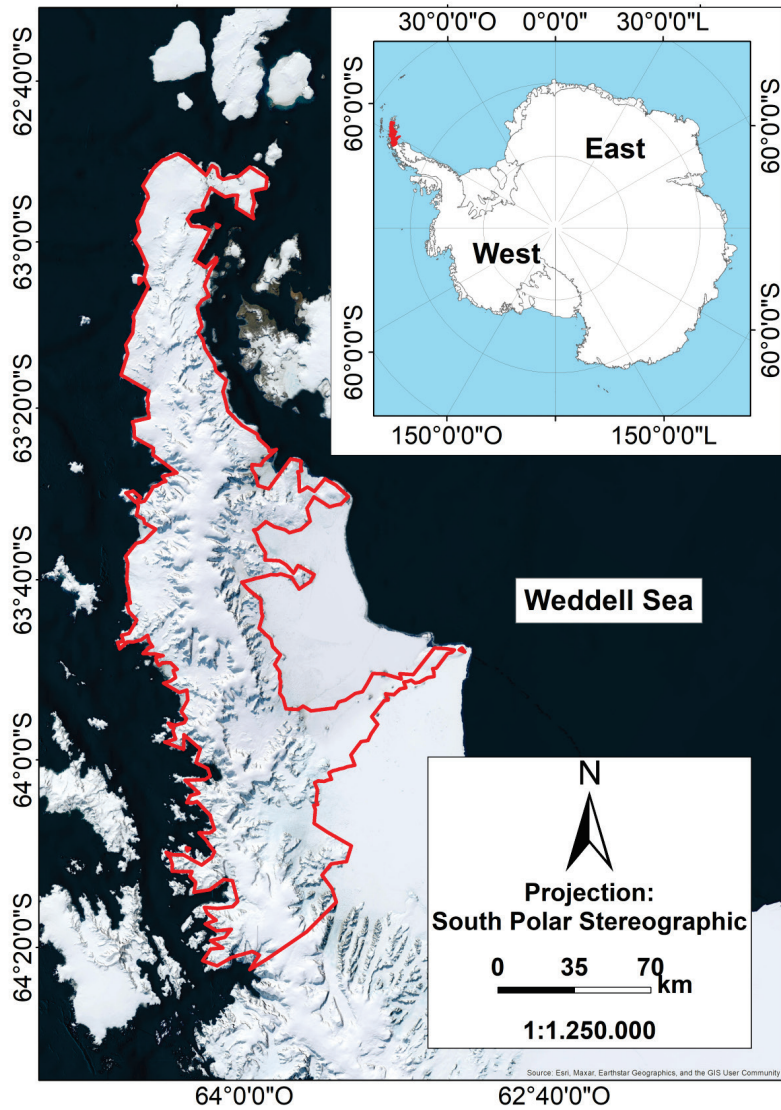


**Figure 1.** Location map of the study area marked in red. Data from Quantarctica and ESRI Imagery 2023.

(GRD) in dB (GEE 2022). This collection offers pre-processed products that have undergone essential processing steps using the European Space Agency’s (ESA) S1 Toolbox (ESA 2021). These steps include applying the orbit file, eliminating thermal noise, removing GRD border noise, performing radiometric calibration to  $\sigma^0$ , and conducting Range-Doppler terrain correction. This pre-processing significantly simplifies the data analysis pipeline, requiring only the consideration of noise effects and radiometric terrain corrections. The data for the

AP were available in Extra Wide (EW, 40 m spatial resolution) and in Interferometric Wide Swath (IW, 10 m spatial resolution) acquisition modes.

CryoSat-2 (CS2) Antarctica 1km DEM is a Digital Elevation Model (DEM) of the Antarctic ice sheet and ice shelves, based on observations recorded between July 2010 and July 2016 by the CS2 radar altimetry satellite (Slater et al. 2018). CS2 is formed from spatiotemporal fits to elevation measurements accumulated in 1, 2, and 5 km grid cells and is available at 1 km spatial resolution. The median and average square

difference between this DEM and the  $2.3 \times 10^7$  airborne laser altimeter measurements acquired during NASA's Operation IceBridge campaigns were -0.30 m and 13.50 m, respectively.

The ERA5 reanalysis meteorological data grid completes the database used in this research. ERA5 is the fifth generation of the European Centre for Medium-Range Weather Forecasts (ECMWF) for global climate and weather over the past four to seven decades. It combines model data with observations worldwide into a globally complete and consistent dataset (ECMWF 2021).

**Methodology**

This paper analyzes variations in the extension of the Dry Snow Radar Zone (DSRZ) and the Wet Snow Radar Zone (WSRZ). These zones can be distinguished from other radar-detected glacier zones by differences in backscatter and altitude characteristics (Zhou et al. 2021). The Lee filter (Mullissa et al. 2021) was applied using a 5x5 pixel moving window to mitigate the speckle effect, and the incidence angles were fixed at  $30^\circ$ . Subsequently, thresholds in backscatter coefficients ( $\sigma^0$ ) were established to identify winter dry snow areas. Herein, regions with  $\sigma^0$  values exceeding -6.5 dB signify the extent of surface melt occurrence (Zhou & Zheng 2017,

Liang et al. 2021, Zhou et al. 2021). Figure 2 shows the processing chain applied in this study.

CS2 was used as the basis for the terrain correction, an auxiliary product for applying altitude masks, correcting the landscape slope in the S1 images, and normalizing the backscatter coefficient on the land. Altitude is also important for identifying different zones on glaciers. The DSRZ is restricted to the upper part of glaciers, and the DSL is considered to coincide with the  $-11^\circ\text{C}$  isotherm of the average annual air temperature, while the wet snow zone is lower than the altitude of this isotherm. An altitude below 500 m is considered as exposed ice. To distinguish DSRZ from WSRZ and exposed ice with similar backscattering characteristics, altitude is the other threshold considered to extract DSL (Rau & Braun 2002, Arigony-Neto et al. 2007, Zhou et al. 2021). Therefore, the limit of 1200 m, 800 m, and 500 m were adopted in the AP ice sheet areas that are included north of  $67.5^\circ\text{S}$ , between  $67.5^\circ\text{S}$  and  $72^\circ\text{S}$ , and south of  $72^\circ\text{S}$ , respectively (Arigony-Neto et al. 2007, Zhou & Zheng, 2017, Zhou et al. 2021). These altitude boundaries were extracted from CS2 in the GEE.

The ERA5 data were specifically processed to provide the mean surface temperature at a 2m height above the surface. These measurements

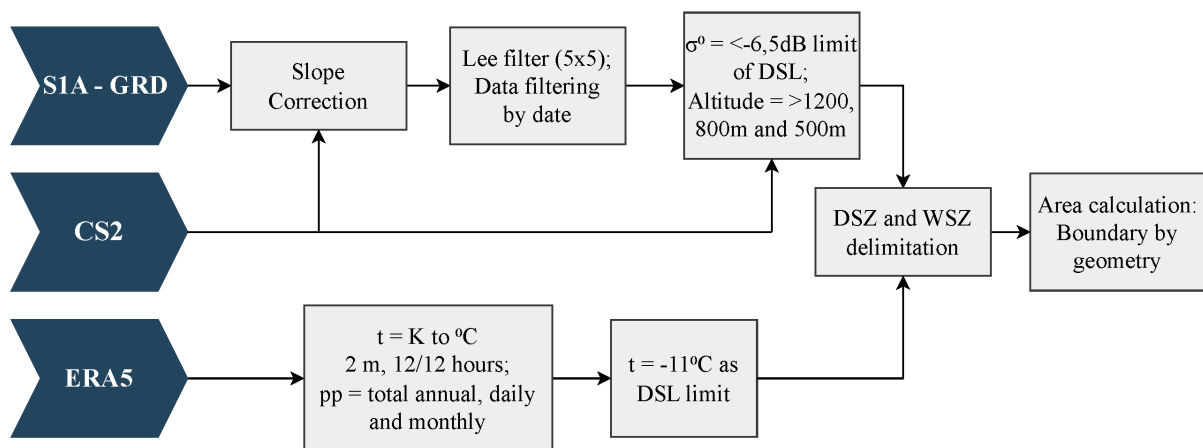


**Figure 2. Processing chain applied in this study.**

were collected and compiled every 12 hours, converting the values from Kelvin to Celsius (°C) and a filter of -11 °C was applied to aid in the interaction of backscatter and altitude. Monthly and annual degree-day sums were estimated from daily and monthly mean temperatures and the information of precipitation was also compiled to obtain total annual and summer precipitation data. The GEE platform was applied to the approach and the Supplementary Material - Code S1 contains the source code utilized in the methodology.

The results were compiled and categorized into data on annual total precipitation, average air temperature, annual degree-day sums and DSRZ and WSRZ area. These datasets were subjected to the Mann-Kendall test, correlation and multivariate analyses. The Mann-Kendall (Mann 1945, Kendall 1957) is one of non-parametric tests most used in the world to detect significant trends in temporal series (Shivam et al. 2019, Machiwal et al. 2019, Dos Santos et al. 2020), which is appropriate to climatic (Goossens & Berger 1986) and another environmental series. To perform a Mann-Kendall test, compute the difference between the later-measured value and all earlier-measured values,  $(y_j - y_i)$ , where  $j > i$ , and assign the integer value of 1, 0, or -1 to positive differences, no differences, and negative differences, respectively (Meals et al. 2011). The test statistic,  $S$ , is then computed as the sum of the integers:

$$S = \sum_{i=1}^{n-1} \sum_{j=i+1}^n \text{sign}(y_j - y_i)$$

Where  $\text{sign}(y_j - y_i)$  is equal to +1, 0, or -1 as indicated above. When  $S$  is a large positive number, later-measured values tend to be larger than earlier values and an upward trend is indicated. When  $S$  is a large negative number, later values tend to be smaller than earlier values and a downward

trend is indicated. When the absolute value of  $S$  is small, no trend is indicated (Meals et al. 2011).

## RESULTS

The DSRZ is restricted to higher elevation land areas where, even in summer, temperatures do not exceed the melting point, preventing surface melting from occurring and maintaining a similar behavior in the backscattering signal (Figure 3). However, in lower areas the WSRZ shows a significant change in the backscatter values between winter and summer (Figure 3), and demonstrates a downward trend (-0.47) in relation to the total degree-day sum.

The WSRZ has varied considerably during the analyzed period, mainly in the 2015-2016 summer, with 9,879.51 km<sup>2</sup>, and in the 2019-2020 summer, with 11,663.61 km<sup>2</sup> of WSRZ (Table I and Figure 4). The 2018-2019 summer had the lowest WSRZ extent, with 6,600.57 km<sup>2</sup> (Table I and Figure 4).

The WSRZ area showed a significant variation in the period analyzed, with a decrease between the summer seasons from 2015/2016 to 2018/2019, and a rise in the summer of 2019/2020, which showed the largest values in our time series (Figure 4). The area size of WSRZ during the summers of 2019/2020, 2020/2021, and 2022/2023 exhibited larger values compared to the area size in 2018/2019. The extension of the WSRZ area has not yet reached the levels observed in 2019/2020 after the 2019/2020 summer. Compared to WSRZ, DSRZ showed a small variation over the analyzed period. The lowest value presented for the DSRZ was 5,494.04 km<sup>2</sup> in 2017-2018, comparable in area with the period 2022-2023, with 5,545.5 km<sup>2</sup>. The highest value was 6,712.82 km<sup>2</sup> in 2021-2022, near 2015-2016 with 6,664.46 km<sup>2</sup> (Table I and Figures 5 and 6). The period 2018-2019 showed the smallest area of WSRZ on the time series (Figure 4 and 6).

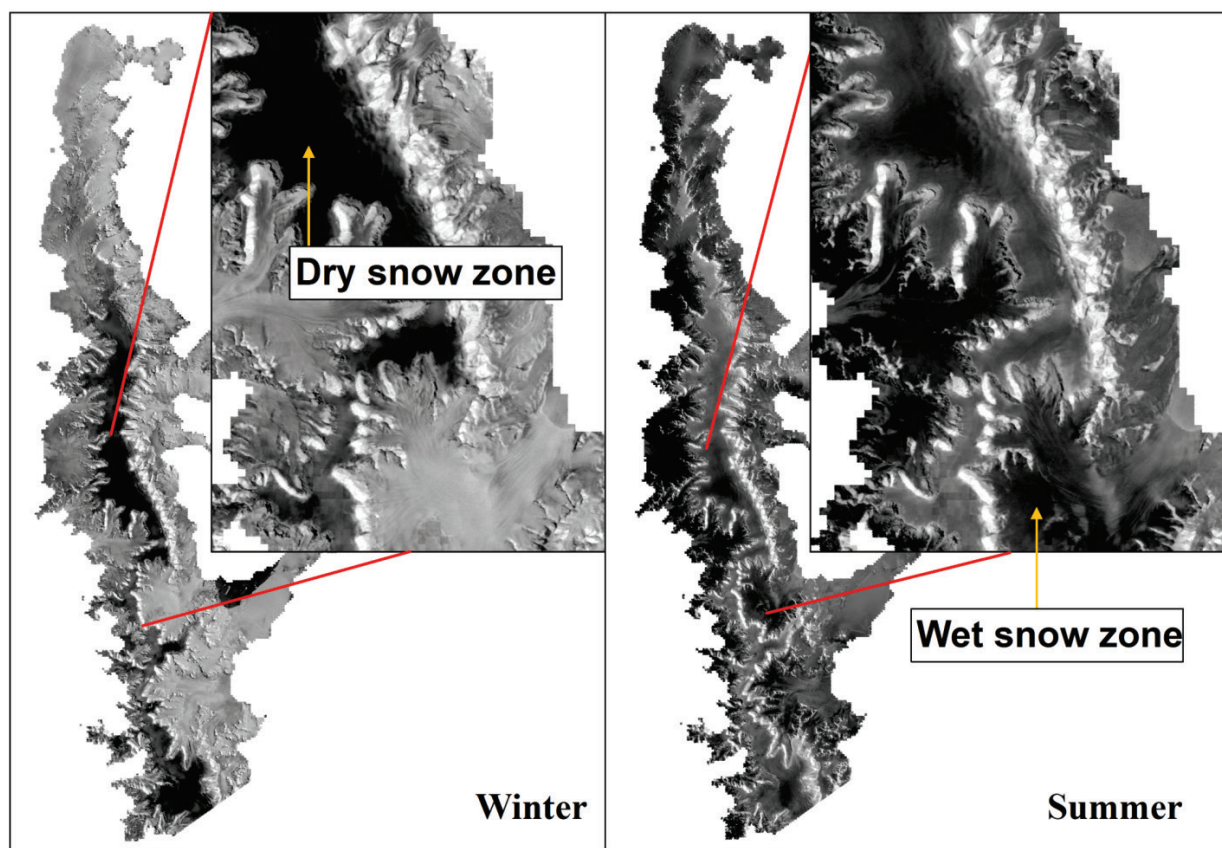


**Figure 3.** Backscatter difference between winter and summer in S1 images. The contrasts of radar signal backscatter enabling visual identification of radar snow zones.

The maximum WSRZ extent has oscillated from 6,600 to 11,663 km<sup>2</sup> since 2015. The temporal change analysis of mean values by period shows a 14.5% mean value increase of WSRZ extent and 0.4% reduction in DSRZ since 2015. The DSRZ showed a slight decrease for the period (Figures 5 and 6). The 2019/2020 and 2020/2021 values are smaller than 2018/2019 for DSRZ, while the 2021/2022 and 2015/2016 values are higher.

The ERA5 data are available from 1981 to the present and show an increasing trend in temperature (Figure 7), which corroborates the results obtained by Carrasco et al. (2021) and Cardoso (2022). In the temporal series, the average air temperature over the period was -9.2 °C, with minimum values of -9.95 °C, in 2014 and -10.4 °C in 2015. The maximum value was

-8.05 °C in 2016. After this year (in 2014 and 2015, the average temperature has an increasing ± 0.096 °C year<sup>-1</sup>).

The 2020 presented the highest values (18 days) of the annual degree-day sums series. The annual degree-day sum's lowest value (0) was recorded in 2018. The monthly degree-day sums showed increasing values from January 2014 to January 2023 (Figures 8 and Table II). The largest occurrences of these temperatures were in February, with 27 days, followed by January, with 25 days, throughout the series (Figure 8).

The historical precipitation series between 1981-2022 (Figure 9) shows that the AP region shows varied values of total precipitation between years, with an average value of 624.51mm, a minimum of 512.31 mm, in 2019,

**Table I. Area distribution of WSRZ and DSRZ in the study area (in km<sup>2</sup>).**

Period	WSRZ - km <sup>2</sup>	DSRZ - km <sup>2</sup>	MOD+ORBT
06/2014 - 02/2015	no images	no images	no images
06/2015 - 02/2016	9879.5	6664.4	IW DESC
06/2016 - 02/2017	8634.1	5494.0	EW ASC
06/2017 - 02/2018	9215.4	5737.3	EW ASC
06/2018 - 02/2019	6600.5	5943.8	EW DESC
06/2019 - 02/2020	11663.6	5756.0	EW DESC
06/2020 - 02/2021	9055.6	5744.2	EW DESC
06/2021 - 02/2022	8873.2	6614.4	EW DESC
06/2022 - 02/2023	9721.5	5545.5	EW DESC

and a maximum of 824.40 mm in 2021. The year 2014 recorded 553.74 mm of total precipitation, although the years 2019 and 2020 were the driest ones. Despite a more than 140 mm decrease between 2021 and 2022, the values also show an increasing of ±13.362 mm.yar-1 in the analysis period (Figure 9).

The annual variation of the WSRZ area in relation to annual air temperature and total precipitation has shown moderate correlations (-0.57 and -0.66), respectively. Similarly, the annual WSRZ area variation has shown a positive correlation ( $r^2=0.63$ ) with the annual degree-days sums (January). Statistical tests revealed low determination coefficients and no significant trend values when examining the relationship between the behavior of the annual DSRZ area and atmospheric variables such as annual average air temperature and total precipitation.

**DISCUSSION**

Air Temperature peaks were verified in the series in the periods with greater WSRZ extents (both 2015-2016 and 2019-2020 summer), as well as the record positive continent temperature

in the AP region of 18.4 °C in February 2020 (WMO 2021). Between 2019 and 2020, the average temperature for the months of January showed a positive change from -4.03 °C to -0.9 °C, coinciding with the period of greatest WSRZ extent in the analysis (Figures 6 and 7), following the increasing in the summer of 2022-2023, in which the average reached -0.83 °C.

January and February have experienced constant increases in average air temperature during the analysis period (Table II), which may directly influence WSRZ measurements, whose maximum extent responds directly to external factors. However, a Mann-Kendall test was conducted at a specific point with an elevation of 570 m, where the concentration of WSRZ occurs, located at 60°52'37.52"W, 64°23'38.25"S. With the exception of the degree-day sum (indicating a moderate downward trend value of -0.47), the test did not reveal strong correlations with the atmospheric variables considered in the study. A more comprehensive statistical analysis on the topic could yield more robust results regarding the relationships between these variables.

Temperature increases and consecutive extreme events have markedly influenced the AP ice masses behavior. Arigony-Neto et al.

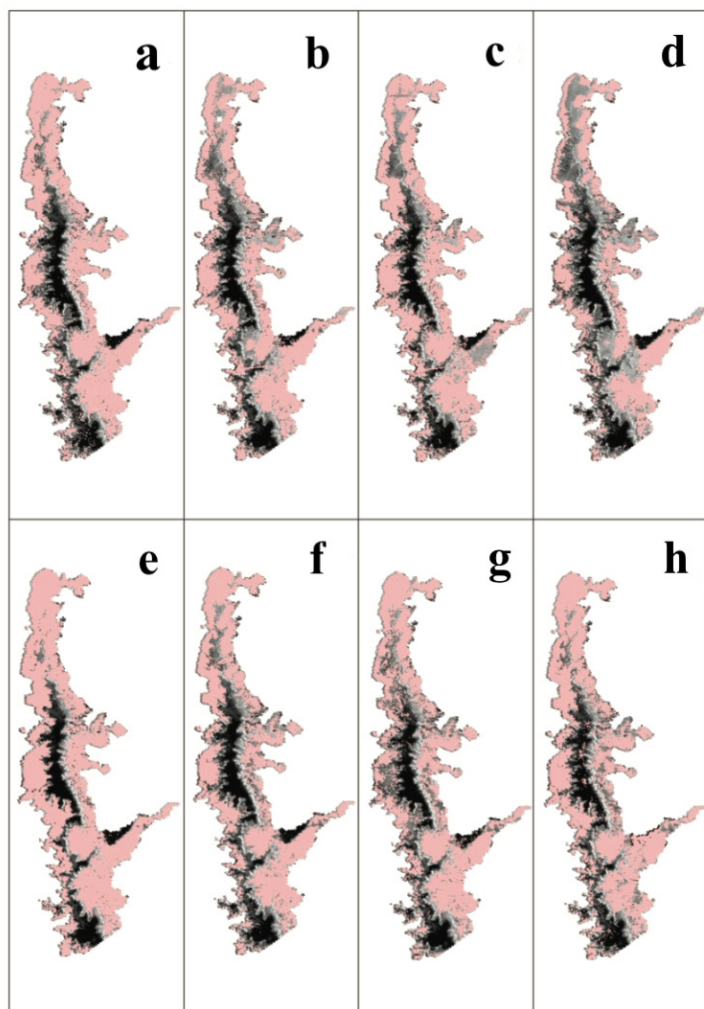


**Figure 4.** Variation of WSRZ in the study area for the periods 2015-2016 (a), 2016-2017 (b), 2017-2018 (c), 2018-2019 (d), 2019-2020 (e), 2020-2021 (f), 2021-2022 (g), and 2022-2023 (h).

(2009) attributed upward changes in the altitude of the dry snow line on the Antarctic Peninsula to extremely high-temperature events impacting the central highlands, and the increased duration of warming periods. Turner et al. (2019) analyzed the correlation between observed annual temperature data from 1979 to 2018 and yearly average sea ice concentrations in AP. They noted a negative sea ice concentration anomaly around Esperanza and Marambio Stations due to the positive air temperature anomaly since 2016.

In addition to variations in January and February demonstrating increasing temperature,

changes were also found for winter month temperatures in the series. The ERA5 data shows an increasing for the months of July in the series and a peak of temperature increase between the years 2015 and 2016 ranging from  $-17.8\text{ }^{\circ}\text{C}$  to  $-13.3\text{ }^{\circ}\text{C}$ , which coincides with higher values in WSRZ extent and lower values in DSRZ extent (Figures 6 and 7). As such, the low values over the series of DSRZ, when compared to the values at the beginning of the series and the end of the series, and the high values of WSRZ could be explained by the positive anomaly of mean air temperature in the region since 2016 (Figures 6 and 7).

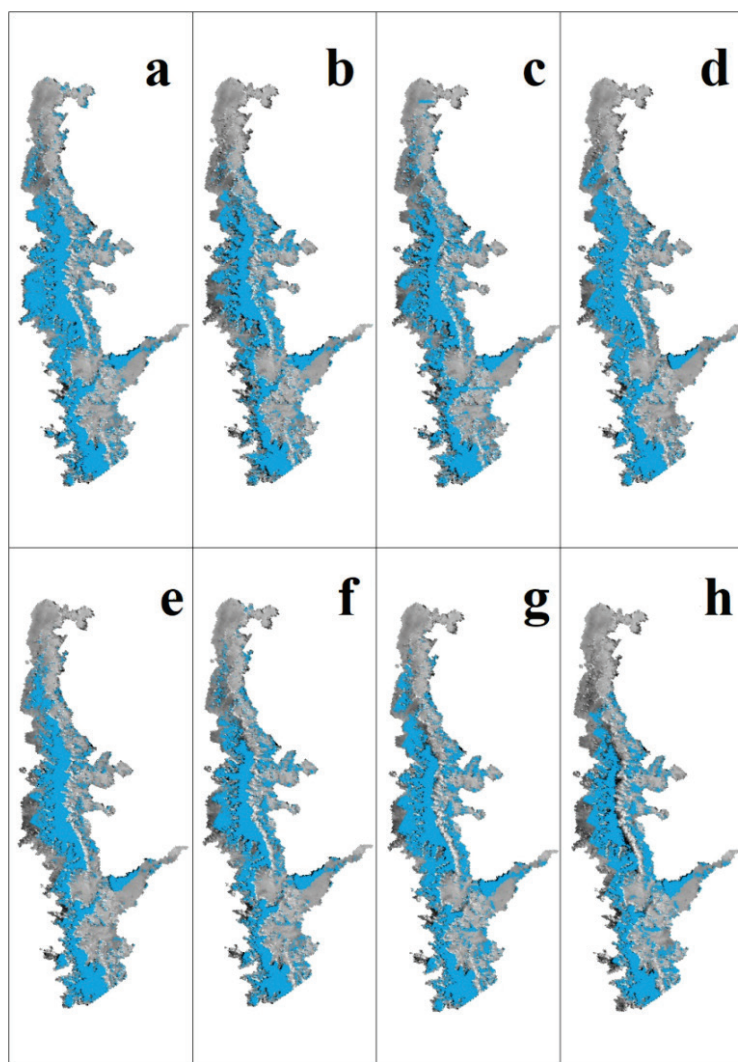


**Figure 5.** Variation of DSRZ in the study area in the periods 2015-2016 (a), 2016-2017 (b), 2017-2018 (c), 2018-2019 (d), 2019-2020 (e), 2020-2021 (f), 2021-2022 (g), and 2022-2023 (h).

On the other hand, DSRZ behavior is also responding to the precipitation variation. The period 2015-2016 showed a higher value of DSRZ than the consecutive years, succeeding a lower annual average air temperature until the year 2015, followed by an increase for 2016 and a slight increase in precipitation in the previous years until 2016, in which it reached a peak of 630.07 mm and then returned to have a drop in values. The low values in DSRZ in 2016 could be explained by the temperature-precipitation relationship according to Bakke & Nesje (2011). After that, in the period 2018-2019, the DSRZ responds to the increases in total precipitation

and air temperature in the year 2018 and again maintains a pattern of lower values until the maximum peak in 2022, which responds to the drier periods between 2018 and 2020 (Figures 6 and 9).

In 2017/2018 and 2018/2019, there was an increase in DSRZ values. The annual mean air temperature has decreased between 2016 and 2017, and between 2018 and 2019 and the WSRZ has a lowest value for 2018/2019 period (Figures 6 and 7). The period 2018-2019 has the smallest WSRZ area and the second largest DSRZ area in the time series, which may be related to the decrease in annual average surface air

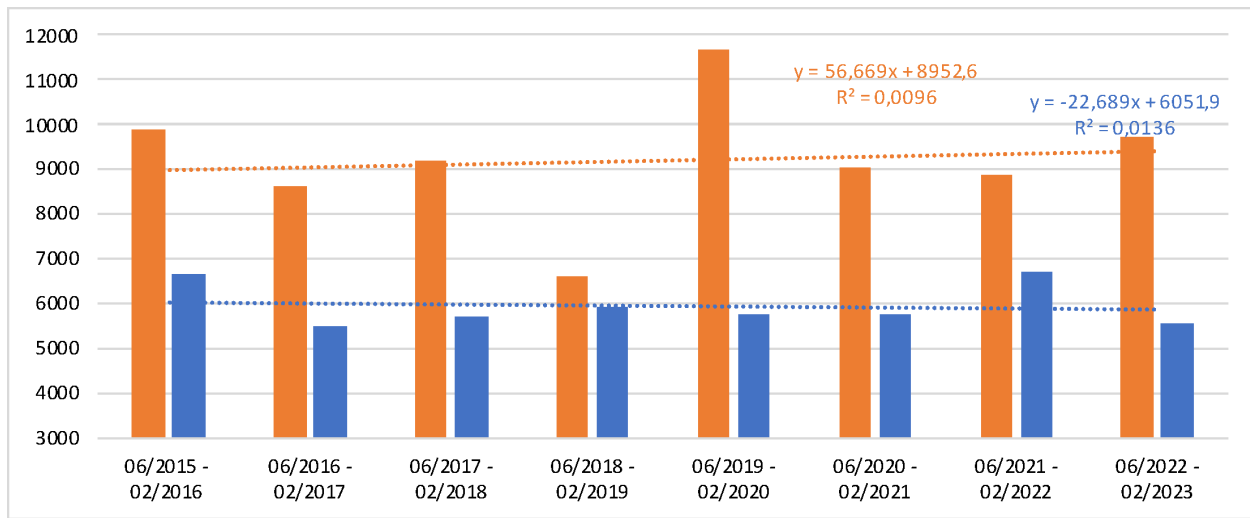


**Figure 6.** Area in km<sup>2</sup> of the WSRZ (orange) and DSRZ (blue) by period. WSRZ did not return to low values like the period of 2018/2019.

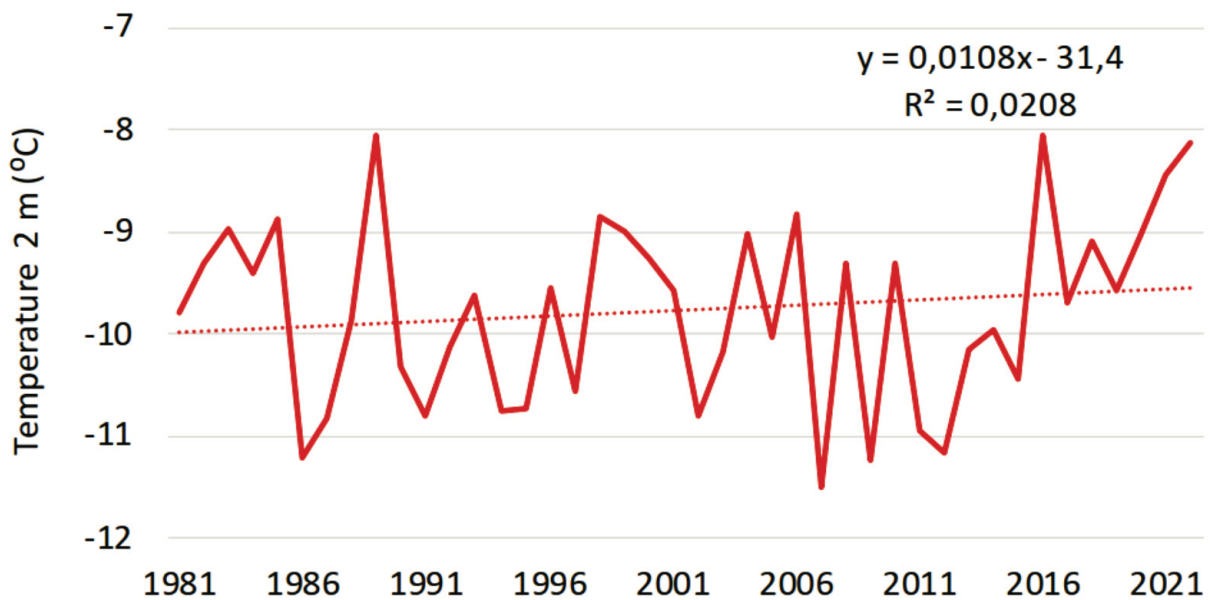


**Figure 7.** ERA5 data for average annual air temperature at 2 m in the study area. The temperature data shows a warming trend of ±0.012 °C year<sup>-1</sup> for the study area.

temperature, as well as having presented a wet July 2018 (when compared to the total annual precipitation values this year to other years in the series, such as 2019 and 2020).

The methodology results show that, despite the variability of occurrence in all years of analysis, there is an increasing area of the WSRZ and decreasing area of the DSRZ, but without a

statistically significant trend. The highest values (18 days) of the annual degree-day sums series in 2020 and air temperature extreme events could be influenced by the smallest area of DSRZ on the time series observed for 2019-2020 and 2020-2021 periods. As the DSRZ is restricted to the uppermost parts of the ice sheets, previous work has evaluated the DSL transition as

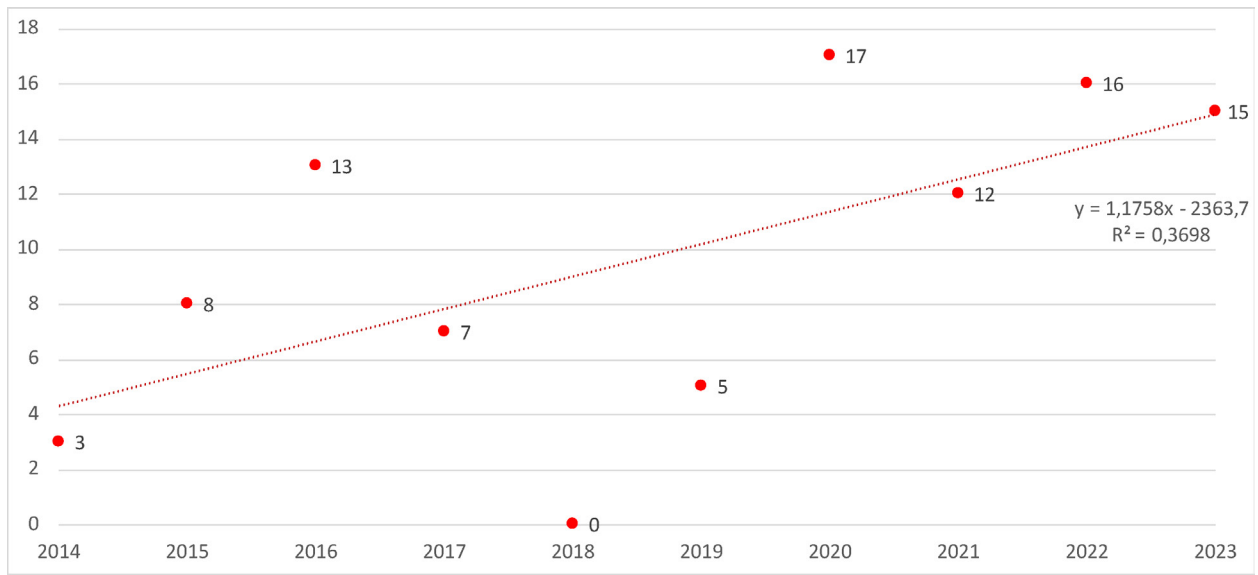


**Figure 8.** Annual degree-day sums between 2014 and 2022-2023. The last 4 years of the period did not present less than 10 days of degree-days sum.

indicative of DSRZ variation using SAR data. Rau & Braun (2002) demonstrated that the observed upward shift of the dry-snow line between 1992 and 1998 is interpreted as a direct result of the increasing number of high-temperature events affecting the DSRZ snow cover and influencing WSRZ variation.

Other works have analyzed radar ice zones in AP and obtained approximate results. Arigony-Neto et al. (2009) demonstrated that the DSL altitude had a widespread increase during 1992-2005 in response to extreme high-temperature events impacting the central highlands of AP, considering the increasing duration of warming periods. This growth in DSL altitude implies a decrease in DSRZ area, restricting it to higher regions. The same paper indicates that an average reduction of dry snow line altitude was detected in the western part of AP, which was identified as a response to increased precipitation and accumulation.

Whereas with the S1 series, the methodology that Zhou & Zheng (2017) applied demonstrated the SAR-derived melt signals and showed that these events have increased in different

proportions and AP areas. The western region of AP has suffered more intense and longer-lasting snow surface melt events which may be fueled by atmospheric effects, such as Föhn winds (Luckman et al. 2014, Zhou & Zheng 2017, Mendes Jr et al. 2022, Zhu et al. 2023). In addition, the DSL

**Table II.** Monthly degree-days sum between 2014-2023. 2023 shows more degree-days than others years when considering only January and February months in the analysis.

YEAR/MONTH	Jan	Feb	Mar	Nov	Dec
2014	3	0	0	0	0
2015	5	1	2	0	0
2016	5	4	3	0	0
2017	2	1	2	2	0
2018	0	0	0	0	0
2019	0	1	0	2	2
2020	9	7	1	0	0
2021	3	8	0	0	1
2022	6	6	0	0	4
2023	10	5			

has experienced increased elevation from south to north, and higher average air temperatures at lower latitudes allow snow melt to reach higher areas.

GEE allows SAR image processing for large land areas quickly after completing the correct script assembly. According to S1A pixel count the portion of the AP analyzed in this study has approximately 17,000.00 km<sup>2</sup>. The average time for running and processing the data in the script ranged from five to ten seconds for obtaining the base information, such as the number of images available and the graphs of temperature and precipitation distribution in the analysis period, and from two to three minutes for obtaining the specific information of wet and dry snow areas.

**CONCLUSIONS**

The advancements enabled by processing large amounts of data on platforms like the Google Earth Engine (GEE) have significantly reduced

time and working conditions compared to using advanced software on dedicated computers for processing. The application of Sentinel-1 data in glacier zone studies has proven to be efficient for analyzing large-scale spatial and temporal variations.

The study provides a comprehensive review of methods previously employed for the analysis of radar snow zones in SAR images. These methods were adapted and implemented on a digital processing platform, streamlining the selection, data processing, and analysis of results on a large temporal scale and with a substantial quantity of analyzed data. This approach facilitated the identification, analysis, and quantification of area variations in the zones. The methodology employed proved to be satisfactory for the treatment of available data, and the results demonstrated its effectiveness for both quantitative and qualitative analyses of data obtained in digital processing environments.

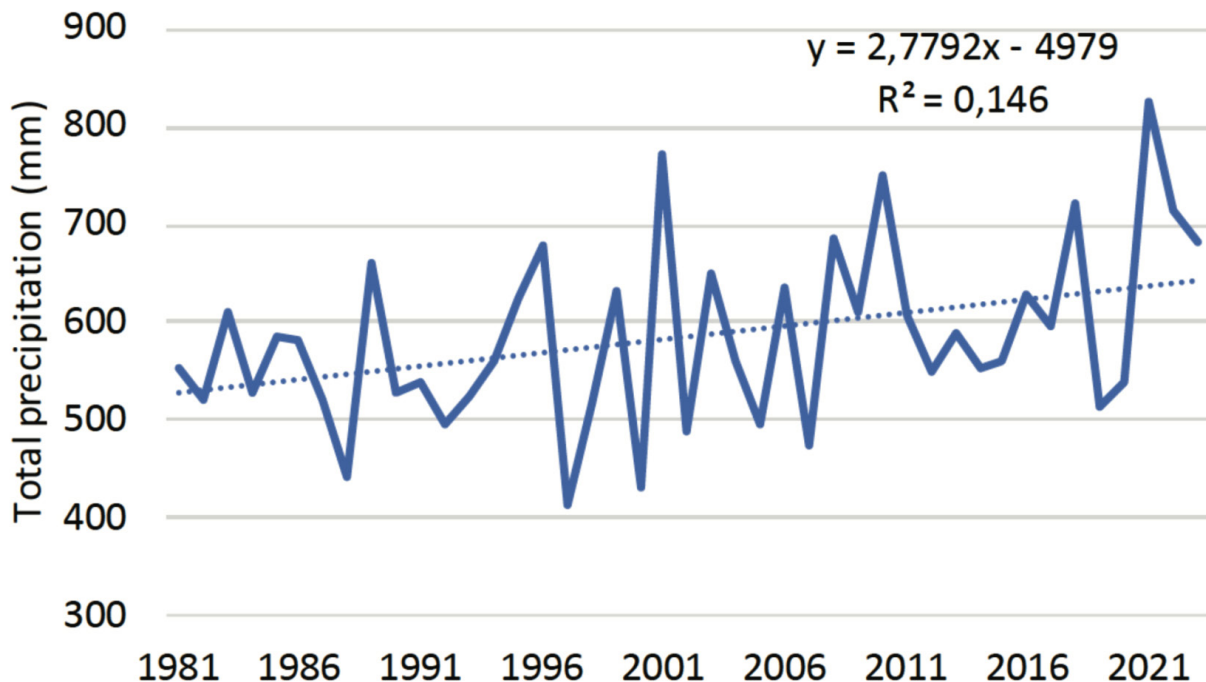


**Figure 9.** Total annual precipitation in the study area. Data by ERA5. The precipitation data series also demonstrates a positive trend of ±1.113 mm.year-1 for the study area.

This technological adaptation makes a complex process more accessible and manipulable.

The area size of WSRZ during the summers of 2019/2020, 2020/2021, and 2022/2023 exhibited the highest values compared to the area size in 2018/2019. The WSRZ area size has not yet reached the levels observed in 2019/2020. The higher values have been related to the summer average air temperature and the annual positive temperature degree days. The annual variation of the dry snow area between the austral winter periods (June to August) showed a slight decrease during 2015-2023 as response to the ongoing Antarctic warming and extreme melt events, as demonstrated in other works (Rau et al. 2001, Arigony et al. 2007, Zhou & Zheng 2017, Mendes Jr et al. 2022).

Driving variables are precipitation and air temperature and elevation. This indicates that other factors should be considered in future analyses for a better understanding of environmental changes, such as atmospheric pressure, drought indices, and the behavior of radar glacier percolation zones. Results of this analysis demonstrate that the proposed methodology can be a valid approach to monitor annual DSRZ and WSRZ extension on a regional scale, such as for the northern portion of AP. It is important to emphasize the utilization of more accurate data in future research on snow zones, including better resolution, extended analysis periods, and reduced data revisit times. These improvements can contribute to a more comprehensive understanding of the behavior of these objects in the study area

### Acknowledgments

We gratefully acknowledge the support of the Centro Polar e Climático (CPC), the Universidade Federal do Rio Grande do Sul (UFRGS), the FAPERGS, and the Conselho Nacional de Desenvolvimento Científico e Tecnológico

(CNPq), Project FAPERGS 21/2551-0002042-3, Project 465680/2014-3 (INCT da Criosfera).

### REFERENCES

- ARIGONY-NETO J, RAU F, SAURER H, JAÑA R, SIMÕES JC, VOGT SA. 2007. Time series of SAR data for monitoring changes in boundaries of glacier zones on the Antarctic Peninsula. *Ann Glaciol* 46: 55-60. Disponível em: [https://www.cambridge.org/core/product/identifier/S0260305500253913/type/journal\\_article](https://www.cambridge.org/core/product/identifier/S0260305500253913/type/journal_article).
- ARIGONY-NETO J, SAURER H, SIMÕES JC, RAU F, JAÑA R, VOGT S & GOSSMANN H. 2009. Spatial and temporal changes in dry-snow line altitude on the Antarctic Peninsula. *Clim Change* 94(1-2): 19-33. <https://doi.org/10.1007/s10584-009-9550-1>.
- BAKKE J & NESJE A. 2011. Equilibrium-Line Altitude (ELA). In: Singh VP, Singh & Haritashya UK (Eds) *Encyclopedia of Snow, Ice and Glaciers*. Encyclopedia of Earth Sciences Series. Springer, Dordrecht. [https://www.google.com/url?q=https://doi.org/10.1007/978-90-481-2642-2\\_140&sa=D&source=docs&ust=1700624873229771&usg=AOvVaw2yPSGtEaNyMEk47wXb9xYh](https://www.google.com/url?q=https://doi.org/10.1007/978-90-481-2642-2_140&sa=D&source=docs&ust=1700624873229771&usg=AOvVaw2yPSGtEaNyMEk47wXb9xYh).
- BEVAN S, LUCKMAN A, HENDON H & WANG G. 2020. The 2020 Larsen C Ice Shelf surface melt is a 40-year record high. *Cryosphere* 14(10): 3551-3564. <https://dx.doi.org/10.5194/tc-14-3551-2020>.
- BUCHELT S, SKOV K & ULLMANN T. 2022. Sentinel-1 time series for mapping snow cover and timing of snowmelt in Arctic periglacial environments: Case study from the Zackenberg Valley, Greenland. *Cryosph Discuss* 16(2): 626-646. <https://dx.doi.org/10.5194/tc-16-625-2022>.
- CARDOSO PS. 2022. Colapso do lago Boeckella, Baía Esperanza: as mudanças nas áreas livres de gelo na Península Antártica. Masters Degree dissertation. Post Graduation Program of Geography, Federal University of Fluminense. Niterói, Rio de Janeiro, 90 p. (Unpublished).
- CARRASCO JF, BOZKURT D & CORDERO RR. 2021. A review of the observed air temperature in the Antarctic Peninsula. Did the warming trend come back after the early 21st hiatus? *Polar Sci* 28: 100653. <https://doi.org/10.1016/j.polar.2021.100653>.
- COOK A J & VAUGHAN DG. 2010. Overview of areal changes of the ice shelves on the Antarctic Peninsula over the past 50 years. *Cryosph* 4(1): 77-98. <https://dx.doi.org/10.5194/tc-4-77-2010>.
- COSTI J, ARIGONY-NETO J, BRAUN M, MAVLYUDOV B, BARRAND NE, DA SILVA AB, MARQUES WC & SIMÕES JC. 2018. Estimating

surface melt and runoff on the Antarctic Peninsula using ERA-Interim reanalysis data. *Antarct Sci* 30(6): 379-393. <https://doi.org/10.1017/S0954102018000391>.

DOS SANTOS TV, FREITAS LA, GONÇALVES RD & CHANG HK. 2020. Teste de Mann-Kendall aplicado a dados hidrológicos – Desempenho dos filtros TFPW e CV2 na análise de tendências. *Ciência e Nat* 42: 87 p. <https://periodicos.ufsm.br/cienciaenatura/article/view/41928>.

ECMWF - EUROPEAN CENTRE FOR MEDIM-RANGE WEATHER FORECASTS. 2021. <https://cds.climate.copernicus.eu/cdsapp#!/dataset/reanalysis-era5-single-levels?tab=overview>.

ESA - EUROPEAN SPACE AGENCY. 2012. Sentinel-1: ESA's radar observatory mission for GMES operational services. ISSN 00344257. ESA Communication, (2012), 96. Available at: <https://earth.esa.int/eogateway/documents/20142/0/Sentinel-1-ESA's-Radar-Observatory-Mission-for-GMES-Operational-Services.pdf>.

ESA - EUROPEAN SPACE AGENCY. 2021. <https://sentinels.copernicus.eu/web/sentinel/technical-guides/sentinel-1-sar/products-algorithms/level-1-algorithms/ground-range-detected>.

FROST VS, STILES JA, SHANMUGAN KS & HOLTZMAN JC. 1982. A Model for Radar Images and Its Application to Adaptive Digital Filtering of Multiplicative Noise. *IEEE Trans Pattern Anal Mach Intell PAMI-4* (2): 157-166. <https://doi.org/10.1109/TPAMI.1982.4767223>.

GEE - GOOGLE EARTH ENGINE. 2022. <https://code.earthengine.google.com/>.

GOOSSENS C & BERGER A. 1986. Annual and seasonal climatic variations over the northern hemisphere and Europe during the last century. *Ann Geophys* 4(4): 385 p.

GORELICK N, HANCHER M, DIXON M, ILYUSHCHENKO S, THAU D & MOORE R. 2017. Google Earth Engine: Planetary-scale geospatial analysis for everyone. *Remote Sens Environ* 202: 18-27. <https://doi.org/10.1016/j.rse.2017.06.031>.

JONES ME, BROMWICH DH, NICOLAS JP, CARRASCO J, PLAVCOVÁ E, ZOU X & WANG SH. 2019. Sixty Years of Widespread Warming in the Southern Middle and High Latitudes (1957-2016). *J Clim* 32(20): 6875-6898. <https://dx.doi.org/10.1175/JCLI-D-18-0565.1>.

KENDALL MG. 1957. Rank Correlation Methods. Oxford University Press 44(1-2): 298, 1957. Available at: <https://www.jstor.org/stable/2333282?origin=crossref>.

LEE JR, RAYMOND B, BRACEGIRDLE TJ, CHADÈS I, FULLER RA, SHAW JD & TERAUDS A. 2017. Climate change drives expansion of Antarctic ice-free habitat. *Nature* 547(7661): 49-54. <https://doi.org/10.1038/nature22996>.

LEE JS. 1980. Digital Image Enhancement and Noise Filtering by Use of Local Statistics. *IEEE Trans. Pattern Anal. Mach. Intell PAMI-2*(2) 165-168. <https://doi.org/10.1109/TPAMI.1980.4766994>.

LI Z, LIU C, ZHANG P & TIAN B. 2018. Assessment of Snow Cover Product Using Google Earth Engine Cloud Computing Platform. In: 2018. IGARSS 2018 - IEEE Int Geosci Remote Sens Symp 5203-5205. <https://doi.org/10.1109/IGARSS.2018.8518931>.

LIANG D, GUO H, ZHANG L, CHENG Y, ZHU Q & LIU X. 2021. Time-series snowmelt detection over the Antarctic using Sentinel-1 SAR images on Google Earth Engine. *Remote Sens Environ* 256(2021): 112318. <https://doi.org/10.1016/j.rse.2021.112318>.

LUCKMAN A, ELVIDGE A, JANSEN D, KULESSA B, MUNNEKE P, KING J & BARRAND E. 2014. Surface melt and ponding on Larsen C Ice Shelf and the impact of föhn winds. *Antarctic Science* 26(6): 625-635. [https://www.cambridge.org/core/product/identifler/S0954102014000339/type/journal\\_article](https://www.cambridge.org/core/product/identifler/S0954102014000339/type/journal_article).

MACHIWAL D, MOHARANA PC, KUMAR S, SRIVASTAVA V & BHANDARI SL. 2019. Exploring Temporal Dynamics of Spatially-Distributed Groundwater Levels by Integrating Time Series Modeling with Geographic Information System. *Geocarto Int* 36: 1325-1345. <https://doi.org/10.1080/10106049.2019.1648561>.

MALENOVSKÝ Z, ROTT H, CIHLAR J, SCHAEPMAN ME, GARCÍA-SANTOS G, FERNANDES R & BERGER M. 2012. Sentinels for science: Potential of Sentinel-1, -2, and -3 missions for scientific observations of ocean, cryosphere, and land. *Remote Sens Environ* 120: 91-101. <https://doi.org/10.1016/j.rse.2011.09.026>.

MANN H B. 1945. Nonparametric tests against trend. *Econometrica* 13(246): 245-259. <https://doi.org/10.2307/1907187>.

MEALS WD, SPOONER J, DRESSING SA & HARCUM JB. 2011. Statistical analysis for monotonic trends. *Tech Notes* 6: 23 p. [https://www.epa.gov/sites/default/files/2016-05/documents/tech\\_notes\\_6\\_dec2013\\_trend.pdf](https://www.epa.gov/sites/default/files/2016-05/documents/tech_notes_6_dec2013_trend.pdf).

MENDES JR CW, ARIGONY-NETO J, HILLEBRAND FL, DE FREITAS MWD, COSTI J & SIMÕES JC. 2022. Snowmelt retrieval algorithm for the Antarctic Peninsula using SAR imageries. *An Acad Bras Cienc* 94: e20210217. <https://doi.org/10.1590/0001-3765202220210217>.

MOUGINOT J, RIGNOTE & SCHEUCHL B. 2014. Sustained increase in ice discharge from the Amundsen Sea Embayment, West Antarctica, from 1973 to 2013. *Geophys Res Lett* 41: 1576-1584. <https://doi.org/10.1002/2013GL059069>.

- MULLISSA A, VOLLRATH A, ODONGO-BRAUN C, SLAGTER B, BALLING J, GOU Y, GORELICK N & REICHE J. 2021. Sentinel-1 SAR Backscatter Analysis Ready Data Preparation in Google Earth Engine. *Remote Sens* 13(10): 1954. <https://doi.org/10.3390/rs13101954>.
- RAU F & BRAUN M. 2002. The regional distribution of the dry-snow zone on the Antarctic Peninsula north of 70° S. *Ann Glaciol* 34: 95-100. <https://doi.org/10.3189/172756402781817914>.
- RAU F, BRAUN M, FRIEDRICH M, WEBER F & GOBMAN H. 2001. Radar glacier zones and their boundaries as indicators of glacier mass balance and climatic variability. *Earsel Procee* 1: 317-327.
- RIGNOT E, MOUGINOT J, SCHEUCHL B, VAN DEN BROEKE M, VAN WESSEM MJ & MORLIGHEM M. 2019. Four decades of Antarctic ice sheet mass balance from 1979-2017. *Proc Natl Acad Sci USA* 116(4): 1095-1103. <https://doi.org/10.1073/pnas.1812883116>.
- SCAMBOS TA, HULBE C, FAHNSTOCK M & BOHLANDERT J. 2000. The link between climate warming and break-up of ice shelves in the Antarctic Peninsula. *J Glaciol* 154: 516-530.
- SHIVAM G, GOYAL MK & SARMA AK. 2019. Index-based study of future precipitation changes over Subansiri river catchment under changing climate. *J Environ Inform* 34(1): 1-14. <https://dx.doi.org/10.3808/jei.201700376>.
- SLATER T, SHEPHERD A, MCMILLAN M, MUIR A, GILBERT L, HOGG A, KONRAD H & PARRINELLO T. 2018. A new digital elevation model of Antarctica derived from CryoSat-2 altimetry. *Cryosph* 12(4): 1551-1562. <https://tc.copernicus.org/articles/12/1551/2018/>.
- STEIG EJ, SCHNEIDER DP, RUTHERFORD SD, MANN ME, COMISO JC & SHINDELL DT. 2009. Warming of the Antarctic ice-sheet surface since the 1957 International Geophysical Year. *Nature* 457(7228): 459-462. <https://doi.org/10.1038/nature07669>.
- SUTTERLEY TC, VELICOGNA I, RIGNOT E, MOUGINOT J, FLAMENT T, VAN DEN BROEKE MR, VAN WESSEM JM & REIJMER CH. 2014. Mass loss of the Amundsen Sea Embayment of West Antarctica from four independent techniques. *Geophys Res Lett* 41(23): 8421-8428. <https://doi.org/10.1002/2014GL061940>.
- THE IMBIE TEAM. 2018. Mass balance of the Antarctic Ice Sheet from 1992 to 2017. *Nature* 558(7709): 219-222. <https://doi.org/10.1038/s41586-018-0179-y>.
- TUCKETT PA, ELY JC, SOLE AJ, LIVINGSTONE SJ, DAVISON BJ, MELCHIOR VAN WESSEM J & HOWARD J. 2019. Rapid accelerations of Antarctic Peninsula outlet glaciers driven by surface melt. *Nat Commun* 10(1): 8 p. <https://doi.org/10.1038/s41467-019-12039-2>.
- TRUSEL LD, FREY KE & DAS SB. 2012. Antarctic surface melting dynamics: Enhanced perspectives from radar scatterometer data. *J Geophys Res* 117: 1-15. <https://doi.org/10.1029/2011JF002126>.
- TRUSEL LD, FREY KE, DAS SB & MUNNEKE PK. 2013. Satellite-based estimates of Antarctic surface meltwater fluxes. *Geophys Res Lett* 40: 6148-6153. <https://doi.org/10.1002/2013GL058138>.
- TURNER J, COLWELL SR, MARSHALL GJ, LACHLAN-COPE TA, CARLETON A M, JONES PD, LAGUN V, REID PA & IAGOVKINA S. 2005. Antarctic climate change during the last 50 years. *Int J Climatol* 25 (3): 279-394. <https://doi.org/10.1002/joc.1130>.
- TURNER J, MARSHALL GJ, CLEM K, COLWELL S, PHILLIPS T & LU H. 2019. Antarctic temperature variability and change from station data. *Int J Climatol* 40(6): 2986-3007. Available at: <https://onlinelibrary.wiley.com/doi/10.1002/joc.6378>.
- VAN DEN BROEKE M. 2005. Strong surface melting preceded collapse of Antarctic Peninsula ice shelf. *Geophys Res Lett* 32: 1-4.
- WANG N, CHEN F, YU B & QIN Y. 2020. Segmentation of large-scale remotely sensed images on a Spark platform: A strategy for handling massive image tiles with the MapReduce model. *ISPRS J Photogramm Remote Sens* 162: 137-147. <https://doi.org/10.1016/j.isprsjprs.2020.02.012>.
- WMO - WORLD METEOROLOGICAL ORGANIZATION. 2021. <https://wmo.int/news/media-centre/wmo-verifies-one-temperature-record-antarctic-continent-and-rejects-another>.
- ZHOU C, LIU Y & ZHENG L. 2021. Satellite-derived dry-snow line as an indicator of the local climate on the Antarctic Peninsula. *J Glaciol* 68(267): 54-64. <https://doi.org/10.1017/jog.2021.72>.
- ZHOU C & ZHENG L. 2017. Mapping Radar Glacier Zones and Dry Snow Line in the Antarctic Peninsula Using Sentinel-1 Images. *Remote Sens* 9(1171): 19 p. <https://doi.org/10.3390/rs911171>.
- ZHU Q, GUO H, ZHANG L, LIANG D, LIU X, ZHOU H & GOU Y. 2023. High-resolution spatio-temporal analysis of snowmelt over Antarctic Peninsula ice shelves from 2015 to 2021 using SAR images. *Int J Digit Earth* 16(1): 825-846. <https://www.tandfonline.com/doi/full/10.1080/17538947.2023.2181991>.

## SUPPLEMENTARY MATERIAL

**CodeS1 -Access link to the code for processing steps on GEE platform:** <<https://code.earthengine.google.com/4ecb93623c9428afdbd61bae3b20afbd>>.

### How to cite

IDALINO FD, ROSA KK, HILLEBRAND FL, ARIGONY-NETO J, MENDES JR CW & SIMÕES JC. 2024. Variability in wet and dry snow radar zones in the North of the Antarctic Peninsula using a cloud computing environment. *An Acad Bras Cienc* 96: e20230704. DOI 10.1590/0001-3765202420230704.

*Manuscript received on June 23, 2023;  
accepted for publication on December 15, 2023*

### FILIPE D. IDALINO<sup>1</sup>

<https://orcid.org/0000-0001-5587-5208>

### KÁTIA K. DA ROSA<sup>1</sup>

<https://orcid.org/0000-0003-0977-9658>

### FERNANDO L. HILLEBRAND<sup>2</sup>

<https://orcid.org/0000-0002-0182-8526>

### JORGE ARIGONY-NETO<sup>3</sup>

<https://orcid.org/0000-0003-4848-2064>

### CLAUDIO WILSON MENDES JR<sup>4</sup>

<https://orcid.org/0000-0003-1745-348X>

### JEFFERSON C. SIMÕES<sup>1</sup>

<https://orcid.org/0000-0001-5555-3401>

<sup>1</sup>Universidade Federal do Rio Grande do Sul, Instituto de Geociências, Centro Polar e Climático, Av. Bento Gonçalves, 9500, 91501-970 Porto Alegre, RS, Brazil

<sup>2</sup>Instituto Federal de Educação Ciência e Tecnologia do Rio Grande do Sul, IFRS, Rodovia RS-239, Km 68, 3505, 95690-000 Rolante, RS, Brazil

<sup>3</sup>Universidade Federal do Rio Grande, Instituto de Oceanografia, Av. Itália, Km 8, 96201-900 Rio Grande, RS, Brazil

<sup>4</sup>Universidade Federal do Rio Grande do Sul, Instituto de Geociências, Centro Polar e Climático, Departamento de Geodésia, Av. Bento Gonçalves, 9500, 91501-970 Porto Alegre, RS, Brazil

Correspondence to: **Filipe Daros Idalino**

E-mail: [idalinofilipe135@gmail.com](mailto:idalinofilipe135@gmail.com)

## Author contributions

This manuscript was elaborated by Filipe Daros Idalino, Fernando Hillebrand, with processes SAR images, climate data, and writing the manuscript. Kátia Kellem da Rosa contributed to the writing and revision. Jorge Arigony-Neto, Claudio Mendes Jr and Jefferson Cardia Simões contribute with discussion of the article's results. All authors reviewed and contribute to the manuscript.

